

# Exceptionally large room-temperature ferroelectric polarization in the novel $\text{PbNiO}_3$ multiferroic oxide.

X.F. Hao<sup>1</sup>, A. Stroppa<sup>2</sup>, S. Picozzi<sup>2</sup>, A. Filippetti<sup>3</sup>, and C. Franchini<sup>1\*</sup>

<sup>1</sup>*Faculty of Physics, University of Vienna and Center for Computational Materials Science, A-1090 Wien, Austria*

<sup>2</sup>*CNR-SPIN L'Aquila, Via Vetoio 10, I-67100 L'Aquila, Italy and*

<sup>3</sup>*CNR-IOM, UOS Cagliari and Dipartimento di Fisica, Università di Cagliari, Monserrato (CA), Italy*

(Dated: August 5, 2021)

We present a study based on several advanced First-Principles methods, of the recently synthesized  $\text{PbNiO}_3$  [J. Am. Chem. Soc **133**, 16920 (2011)], a rhombohedral antiferromagnetic insulator which crystallizes in the highly distorted  $R3c$  crystal structure. We find this compound electrically polarized, with a very large electric polarization of  $\sim 100 \mu\text{C}/\text{cm}^2$ , thus even exceeding the polarization of well-known  $\text{BiFeO}_3$ .  $\text{PbNiO}_3$  is a proper ferroelectric, with polarization driven by large Pb-O polar displacements along the [111] direction. Contrarily to naive expectations, a definite ionic charge of 4+ for Pb ion can not be assigned, and in fact the large Pb 6s-O 2p hybridization drives the ferroelectric distortion through a lone-pair mechanism similar to that of other Pb- and Bi-based multiferroics.

PACS numbers: 77.80.-e, 77.84.-s, 77.22.Ej, 71.20.-b

*Introduction* Multiferroics are materials in which different ferroic orders such as ferromagnetism, ferroelectricity and/or ferroelasticity may coexist in one single phase [1]. In the last few years, there has been a tremendous boom of interest in these materials, due to the potential applications in memory devices or in novel type of magnetic switching in magnetoelectric multiferroics, based on the cross-coupling between ferroelectric and magnetic channels [2–4]. Furthermore, these materials offer a rich and fascinating playground for the complex physical mechanisms underlying the processes involved in the observed properties.[5] It is obvious that the search and the prediction by material design of new multiferroics is of great importance for both fundamental physics and technological applications [6, 7].

Relatively few multiferroics have been identified so far. [8] Without doubt, the most studied and well characterized multiferroic is  $\text{BiFeO}_3$  [9]. It crystallizes in the polar space group  $R3c$  (No. 161, point group  $C_{3v}$ ), and is predicted to have a G-type antiferromagnetic (AFM) alignment of the Fe spins [6, 11]. The  $R3c$  symmetry corresponds to the so-called  $\text{LiNbO}_3$ -type structure, which can be viewed as a highly distorted double perovskite with rhombohedral symmetry. The primitive unit cell contains two formula units (10-atoms), arising from counterrotations of neighboring O octahedra about the [111] axis (see Fig.1). The crystal symmetry allows the presence of a spontaneous polarization along the [111] direction, which arise from the relative displacement of the Bi sublattices with respect to the  $\text{FeO}_6$  octahedra cages along [111]. The origin of the large spontaneous polarization of  $\text{Bi}^{+3}\text{Fe}^{+3}\text{O}^{-2}_3$ ,  $\sim 90 \mu\text{C}/\text{cm}^2$  [9], has been explained by first principles calculations within the density functional theory plus Hubbard-U approach (DFT+U)[19] and the "modern theory of polarization" (MTP) [27, 32], in terms of the lone-pair electrons present at the Bi sites which are ultimately responsible for the

large displacement along the [111] direction [6].

Inspired by the recent reports of Inaguma *et al.* on the synthesis of a new antiferromagnetically ordered compound with  $\text{LiNbO}_3$ -type structure, such as  $\text{PbNiO}_3$ [12, 13], we explore here the possibility of multiferroic behavior in  $\text{PbNiO}_3$ . We first summarize the experimental findings. Inaguma and coworkers synthesized two high-pressure polymorphs of  $\text{PbNiO}_3$  with a (A) perovskite-type structure and (B) the  $\text{LiNbO}_3$ -type structure [12, 13]; the latter (hereafter called L- $\text{PbNiO}_3$ ) is thermodynamically more stable than the perovskite-type one at ambient pressure. With respect to the orthorhombic structure, in the acentric rhombohedral  $\text{LiNbO}_3$ -type ( $R3c$ ) structure (Fig. 1) Pb and O atoms are displaced against each other along the threefold [111] axis leading to a large distortion of the  $\text{PbO}_6$  and  $\text{NiO}_6$  octahedra (see Fig.1). The Pb atom is coordinated by six oxygens at 2.10 and 2.25 Å, while the Ni-O bond distance splits into two subgroups (2.07 and 2.11 Å). Magnetic susceptibility and resistivity measurements indicate that L- $\text{PbNiO}_3$  undergoes an AFM transition at  $T_N=205^\circ\text{K}$ , and exhibits semiconducting behavior. The AFM ordering in the acentric crystal structure suggests possible multiferroic behavior.

In the following we show that L- $\text{PbNiO}_3$  is a *new* room-temperature *multiferroic*, with an *exceptionally large* polarization ( $\mathbf{P}$ ) of about  $100 \mu\text{C}/\text{cm}^2$ , which is the highest polarization ever predicted for any bulk material so far, and  $\approx 10\%$  larger than that of  $\text{BiFeO}_3$  [9].

*Computational details* We performed DFT based calculations using the Vienna *Ab initio* Simulation Package (VASP) [16] based on the projector-augmented-wave method[17, 18], withing the Perdew, Burke and Ernzerhof (PBE) parameterization scheme[15] for the generalized gradient approximation (GGA). To overcome the deficiencies of standard exchange-correlation approximations for localized Ni *d* states, we made use of three

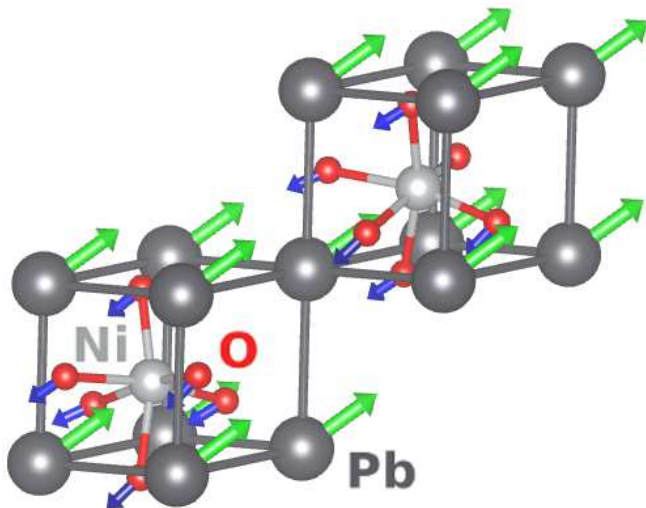


FIG. 1: (Color online) Schematic view of the LiNbO<sub>3</sub>-type PbNiO<sub>3</sub> within space group  $R\bar{3}c$  structure built up from two cubic perovskite unit cells, the black (large), gray (medium) and red (small) spheres denotes Pb, Ni and O atoms, respectively. With respect to the centrosymmetric ( $R\bar{3}c$ ) paraelectric phase (see text) the cations are displaced along the [111] axis relative to the anions (the arrows represent the displacement vectors), and the oxygen octahedra slightly rotate with alternating sense around the [111] direction [12]. The crystal structure was drawn using the program VESTA[14].

beyond-DFT approaches: (i) Dudarev’s GGA+U [19, 20], using  $U=4.6$  eV in accordance with constrained DFT calculation of Ref.21; (ii) The renowned Heyd-Scuseria-Ernzerhof (HSE) screened hybrid functional [22], which has been shown to give an excellent account of materials properties for magnetic multiferroics[23]. (iii) The recently introduced variational pseudo self-interaction-correction method VPSIC[24] (adopting the HSE optimized structure), implemented within plane-wave basis set and ultrasoft pseudopotential scheme in the PWSIC code. The cutoff energy was set as 600 eV and a  $8\times 8\times 8$  Monkhorst-Pack grid of  $k$  points was used. In HSE, the fraction (1/4) of Fock exchange was sampled using the twofold reduced  $k$ -point grid, to reduce the computational load. The lattice parameters and atomic positions were relaxed (at GGA+U and HSE level) until the total energy changed by less than  $10^{-5}$  eV per unit cell and the residual force was smaller than 0.01 eV/Å.

*Magnetic, structural and electronic properties* The G-type antiferromagnetic configuration (AFM-G), in which each Ni ion is surrounded by six nearest-neighbors Ni with opposite spin direction, is the most favourable spin configuration with respect to ferromagnetic (by 50 meV/f.u.), AFM type-A (by 33 meV/f.u.) and AFM type-C (by 17 meV/f.u.) orderings.

The resulting calculated magnetic Ni magnetic moment ( $m_{\text{Ni}}$ ) is about  $1.7 \mu_{\text{B}}$  at both GGA+U and HSE level. The optimized GGA, GGA+U and HSE structural

TABLE I: Structural parameters, magnetic moment and electronic band gap for AFM-G configuration of L-PbNiO<sub>3</sub> within GGA, GGA+U and HSE method, compared with the available experimental data.  $a$ ,  $c$  are the lattice parameters in the hexagonal setting, whereas  $x$ ,  $y$ , and  $z$  are the internal atomic positions of Pb and O. Ni ions sit in the ( $6a$ ) (0,0,0) positions. Bond lengths of Pb–O and Ni–O are also reported.  $\widehat{\text{Ni-O-Ni}}$  ( $^\circ$ ) is the Ni–O–Ni angle.  $m$  indicates the magnetic moment of Ni.

	GGA	GGA+U	HSE	Expt.
$a$ (Å)	5.442	5.430	5.359	5.363
$c$ (Å)	13.737	14.353	14.209	14.090
$z_{\text{Pb}}$	0.2226	0.2885	0.2898	0.2864
$x_{\text{O}}$	0.0605	0.0532	0.0468	0.0487
$y_{\text{O}}$	0.2598	0.3543	0.3579	0.3657
$z_{\text{O}}$	0.0931	0.0702	0.0687	0.0668
Ni–O (Å)	2.051	2.128	2.119	2.109
	1.905	2.060	2.053	2.071
Pb–O (Å)	2.395	2.310	2.258	2.246
	2.238	2.174	2.121	2.104
$\widehat{\text{Ni-O-Ni}}$ ( $^\circ$ )	147.8	140.6	138.1	136.7
$m_{\text{Ni}}$ ( $\mu_{\text{B}}$ )	0.97	1.67	1.69	—
gap (eV)	Metallic	0.37	1.18	—

parameters for the AFM-G phase are listed in Table I. As expected, GGA does not reproduce well the experimental values, whereas HSE and, to a lesser extent GGA+U, deliver numbers in good agreement with experiment, with relative errors of 1.5-2 % (GGA+U) and  $< 1.0\%$  (HSE).

The drawbacks of conventional GGA are more dramatic for the electronic properties. The GGA scheme finds a metallic character, in clear disagreement with experiment [12]. Conversely, the inclusion of either the on-site  $U$  or the Fock exchange cures this limitation and correctly predicts an insulating state with an energy gap of  $\sim 0.4$  eV (GGA+U) and  $\sim 1.2$  eV (HSE), as inferred from the density of states (DOS) shown in Fig.2 (the VPSIC gap is 0.9 eV, see Supplementary Materials (SM)). The gap opens between occupied Ni  $d$  and O  $p$  states, and the lowest unoccupied electronic states that are made up by a mixture of Pb  $s$  and O  $s$  states.

Spin polarization does not affect Pb and O DOS, whereas the Ni atoms display a magnetic moment of  $1.69 \mu_{\text{B}}$ . In hexagonal coordinates (with  $z$  parallel to the [111] direction) the Ni  $d$  states are distributed into two doublets, ( $d_{xy}$ ,  $d_{x^2-y^2}$ ) and ( $d_{xz}$ ,  $d_{yz}$ ), which contribute to the net magnetization by 0.65 and  $1.65 \mu_{\text{B}}$ , respectively, and a spin-degenerate  $d_{z^2}$  singlet (see SM for an  $lm$ -projected DOS). The broad Ni  $3d$  valence manifold is strongly hybridized with the O  $2p$  states, and lies in the energy range between -6 eV and the Fermi level.

The most important feature of the DOS is at the bottom of the valence region, between -9 eV and -6 eV: a large region dominated by highly-hybridized Pb  $6s$  and O  $2p$  states. The presence of a substantial amount of

charge (about 1 electron, see SM) within the Pb 6s orbital is at odds with the nominal  $\text{Pb}^{4+}$  valence originally assumed in the interpretation of X-ray photoemission spectroscopy (XPS) results[12, 13]. In realistic calculations, substantial deviation between the static charges and the nominal ionic charges (due to large hybridization effects) is the rule rather than the exception, thus it certainly does not come as a surprise. In this case, however, this deviation is worthy to be emphasized, since, as we will show below, it is strictly connected to the ferroelectric instability. To highlight the role of Pb 6s-O 2p hybridization, in Fig.2 we show the DOS for the centrosymmetric, non-polar reference structure  $R\bar{3}c$  as well as the polar structure: the major difference is indeed the 2 eV downshift and the broadening (more than a factor-2 bandwidth expansion) of Pb 6s-O 2p spectral weight occurring along with the centrosymmetric-to-ferroelectric transformation. This so-called stereochemical activity of the A-site cation [28, 29] is quite consistent with what occurs in Bi-based ( $\text{BiFeO}_3$ [6],  $\text{BiMnO}_3$ [28, 29]) and Pb-based ( $\text{PbTiO}_3$ [30]) compounds, usually labelled as lone-pair ferroelectrics. (see SM for a more detailed description of the bonding picture in  $\text{PbNiO}_3$  and a one-to-one comparison with the  $\text{BiFeO}_3$  case). This is also reflected in the structural distortions which *predominantly* involve counterdisplacements of Pb and O atoms along the [111] direction (see Fig.1).

In the following we explore the ferroelectric properties of L- $\text{PbNiO}_3$  by evaluating the spontaneous macroscopic polarization  $\mathbf{P}$ . [6].

#### Analysis of ferroelectric polarization

By pseudosymmetry analysis[31] we determine a parent centrosymmetric structure ( $R\bar{3}c$ ) with minimal supergroup symmetries, from which the observed non-centrosymmetric structure can be reached through a continuous structural distortion. By definition, the polarization is zero (modulo a polarization quantum[27, 32]) in this paraelectric (PE) phase ( $\lambda = 0$ ), thus it represents a viable reference state for the evaluation of the polarization in the polar structure ( $\lambda = 1$ ). Here  $\lambda = 1$  is the amplitude of the polar distortion which progressively transforms the  $R\bar{3}c$  phase into the  $R3c$  one. For consistency, we assume for the  $R\bar{3}c$  phase the same volume and rhombohedral angle of the polar structure.

In the PE phase, Pb and O atoms lie in (111)  $\text{PbO}_3$  planes. Symmetry mode analysis shows that the  $\lambda = [0, 1]$  transformation (showed by arrows in Fig.1) is almost exclusively composed by in-phase [111]-parallel relative shift of Pb and O atoms (i.e. a nearly-exclusive  $\Gamma_2^-$ -mode transformation), with some very residual O-rotation contribution. The Pb atoms are displaced from their positions by 0.56 Å and the O atoms by 0.23 Å, while Ni atoms are almost unchanged. This transformation produces an alternate shrinking and dilatation of Pb-O distances along [111] of about 0.8 Å, whereas Ni (111) planes are left off-centered by 0.17 Å with respect

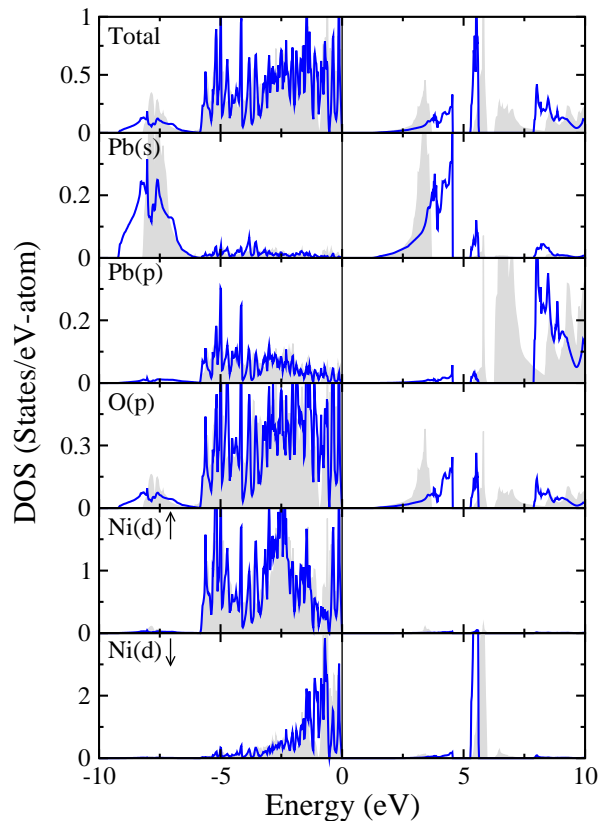


FIG. 2: (Color online) HSE calculated total and site-decomposed density of states for the AFM-G type  $\text{PbNiO}_3$  in the acentric  $R3c$  (full lines) and centric  $R\bar{3}c$  (shadow) phases. The vertical line denotes to the Fermi level.

to their adjacent  $\text{PbO}_3$  planes. The total polarization  $\mathbf{P}$  can be split as the sum of ionic  $\mathbf{P}_{ion}$  and electronic contribution  $\mathbf{P}_{ele}$ : the former is the dipole of the ion-core charges; the latter is obtained by Berry phase approach within the MTP [27, 32]. HSE and VPSIC describe both polar and nonpolar structures as insulating, whereas within GGA+U a large  $U=7.6$  eV is required to open a gap in the PE phase. The HSE-calculated DOS shown in Fig.2 indicates that the value of the gap is essentially the same for both acentric  $R3c$  and nonpolar  $R\bar{3}c$  phases. Fig. 3 displays total energy and polarization  $\mathbf{P}_{tot}$  as a function of the polar distortion  $\lambda$  at both HSE and PBE+U level. Both methods deliver the same outcome. As expected the polar structure is more stable than the non-polar one by 0.6 eV/f.u. (0.7 eV/f.u. according to VPSIC). Both  $\mathbf{P}_{ion}$  and  $\mathbf{P}_{ele}$  grow monotonically with the polar distortion, giving rise to a total polarization  $\mathbf{P}_{tot}$  of  $\sim 100 \mu\text{C}/\text{cm}^2$  ( $98.5 \mu\text{C}/\text{cm}^2$  according to VPSIC), thus  $\approx 10\%$  larger than that of  $\text{BiFeO}_3$  [6, 23] and significantly enhanced with respect to that of  $\text{LiNbO}_3$  ( $80 \mu\text{C}/\text{cm}^2$ )[11] and  $\text{ZnSnO}_3$  ( $57 \mu\text{C}/\text{cm}^2$ )[33].

We have also evaluated the polarization using the approximated expression  $\mathbf{P}_{tot} = \sum_i \Delta R_i Z_i^*$ , where  $\Delta R_i$  are atomic displacements (from centrosymmetric

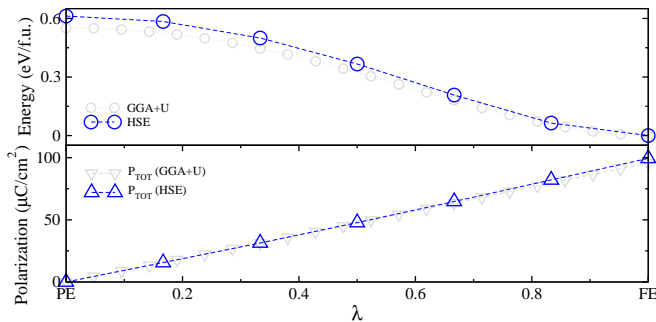


FIG. 3: (Color online) Total energy profile  $E$ , total polarization  $\mathbf{P}_{\text{tot}}$  as a function of the polar distortion  $\lambda$ , from the  $\lambda=0$  PE phase to the  $\lambda=1$  ferroelectric (FE) one. Both HSE (dashed lines, dark) and GGA+U (dotted lines, gray) data are displayed.

to polar structure) and  $Z_i^*$  are Born effective charges (BEC) calculated via linear-response formalism in GGA+U. We obtain a value ( $93.8 \mu\text{C}/\text{cm}^2$ ) substantially similar to the evaluation based on the exact Berry phase formula. We found a nearly isotropic BEC tensor and dynamical charges similar in both PE and FE phases (see Tab.II). For Pb we obtain an anomalous BEC value of 4.4 (as compared to the static charge,  $\approx 2.15$ ), identical to the Bi BEC calculated in  $\text{BiFeO}_3$ , coherently with the role of this ion in guiding the ferroelectric transition[9].

*Summary* Using several beyond-LDA methods (LDA+U, HSE, and VPSIC) and the MTP approach for the determination of polarization properties, we report the presence of a large spontaneous electric polarization  $\sim 100 \mu\text{C}/\text{cm}^2$  in rhombohedral  $\text{PbNiO}_3$  associated to the structural transformation from the centrosymmetric  $R\bar{3}c$  to the polar  $R3c$  symmetry. The microscopic analysis shows that this proper ferroelectric instability is dominated by huge in-phase (i.e.  $\Gamma$ -mode) relative displacements of Pb and on-top O atoms along the [111] direction, in turn associated to large Pb  $s$ -O  $p$  band rehybridization at the bottom of valence band manifold. This ferroelectric mechanism can be then assimilated to other Bi-based and Pb-based ferroelectrics, whereas the naive interpretation of Pb as an inactive +4-charged ion would be totally misleading. This material may be prototype of a new class of Ni-based rhombohedral multiferroics, which take advantage of the stable rhombohedral symmetry to develop large ferroelectric displacements along the [111] axis, and still maintain strong magnetic coupling in the Ni sublattice.

### Acknowledgements

Support by European Community (FP7 EU-INDIA grant ATHENA and ERC Starting Grant no.203523 BIS-MUTH) is gratefully acknowledged. X.H. thanks Claude Ederer and Chung-Yuan Ren for their helpful advices

TABLE II: Born effective charges for Pb and Ni in  $\text{PbNiO}_3$  (with ferroelectric and paraelectric phases) computed via linear-response formalism within the GGA+U method.

	Pb	Ni	O
$R\bar{3}c$ (FE)	4.40	1.97	-2.12
$R\bar{3}c$ (PE)	4.41	1.97	-2.12

and comments. A.S. thanks J.M. Perez-Mato for useful discussions. The calculations have been performed on the Vienna Scientific Cluster (VSC) and, partially, in CASPUR Supercomputing Center in Rome.

\* Corresponding author:cesare.franchini@univie.ac.at

- [1] D. I. Khomskii, *Physics*, **2**, 20 (2009).
- [2] T. Kimura *et al.*, *Nature* **426**, 55 (2003).
- [3] N. Hur, S. Park, P. A. Sharma, J. S. Guha and S. -W. Cheong, *Nature* **429**, 392 (2003).
- [4] S. -W. Cheong and M. Mostovoy, *Nat. Mater.* **6**, 13 (2007).
- [5] I. B. Bersuker, *Phys. Rev. Lett.* **108**, 137202 (2012).
- [6] J. B. Neaton, C. Ederer, U. V. Waghmare, N. A. Spaldin and K. M. Rabe, *Phys. Rev. B* **71**, 014113 (2005).
- [7] C. J. Fennie, *Phys. Rev. Lett.* **100**, 167203 (2008).
- [8] N. A. Hill, *J. Phys. Chem. B* **104**, 6694 (2000).
- [9] J. Wang *et al.*, *Science* **299** 1719 (2003).
- [10] A. M. Glass and M. E. Lines, *Phys. Rev. B* **13**, 180 (1976).
- [11] M. Veithen and Ph. Ghosez, *Phys. Rev. B* **65**, 214302 (2002).
- [12] Y. Inaguma *et al.*, *J. Am. Chem. Soc.* **133**, 16920 (2011).
- [13] Y. Inaguma *et al.*, *J. Phys.: Conf. Ser.* **215**, 012131 (2010).
- [14] K. Momma, F. Izumi, *J. Appl. Crystallogr.* **41**, 653 (2008).
- [15] J. P. Perdew, K. Burke and M. Ernzerhof, *Phys. Rev. Lett.* **77**, 3865 (1996).
- [16] G. Kresse and J. Hafner, *Phys. Rev. B* **48**, 13115 (1993); G. Kresse and J. Furthmüller, *Comput. Mater. Sci.* **6**, 15 (1996).
- [17] P.E. Blöchl, *Phys. Rev. B* **50**, 17953 (1994).
- [18] G. Kresse and D. Joubert, *Phys. Rev. B* **59**, 1758 (1999).
- [19] V. I. Anisimov, F. Aryasetiawan and A. I. Lichtenstein, *J. Phys. Condens. Matter* **9**, 767 (1997).
- [20] S. L. Dudarev, G. A. Botton, S. Y. Savrasov, C. J. Humphreys and A. P. Sutton, *Phys. Rev. B* **57** 1505, (1998).
- [21] M. Cococcioni and S. de Gironcoli, *Phys. Rev. B* **71**, 035105 (2005).
- [22] J. Heyd, G. E. Scuseria and M. Ernzerhof, *J. Chem. Phys.* **118**, 8207 (2003); J. Heyd, G. E. Scuseria and M. Ernzerhof, *J. Chem. Phys.* **124**, 219906 (2006).
- [23] A. Stroppa, S. Picozzi *Phys. Chem. Chem. Phys.* **12** 5405 (2010).
- [24] A. Filippetti, S. D. Pemmaraaju, S. Sanvito, P. Delugas, D. Puggioni, V. Fiorentini, *Phys. Rev. B* **84**, 195127 (2011).
- [25] D.O. Scanlon *et al.*, *Phys. Rev. Lett.* **107**, 246402 (2011).

- [26] G.W. Watson and S. C. Parker, G. Kresse, Phys. Rev. B **59**, 8481 (1999).
- [27] R. D. King-Smith and D. Vanderbilt, Phys. Rev. B **47**, 1651 (1993); D. Vanderbilt and R. D. King-Smith, Phys. Rev. B **48**, 4442 (1993).
- [28] R. Seshadri and N. A. Hill, Chem. Mater. **13** 2892 (2001).
- [29] N. A. Hill and K. M. Rabe Phys. Rev. B **59** 8759 (1999).
- [30] R.E. Cohen, Nature **358**, 136 1992.
- [31] M. I. Aroyo *et al.*, Zeitschrift fuer Kristallographie **221**, **15** (2006); M. I. Aroyo *et al.*, Acta Cryst. **A62**, 115 (2006).
- [32] R. Resta, Rev. Mod. Phys. **66**, 899 (1994).
- [33] M. Nakayama, M. Nogami, M. Yoshida, T. Katsumata and Y. Inaguma, Adv. Mater. **22**, 2579 (2010).